Molecular Therapy
Oncolytics
Original Article

HLA-A*02-gated safety switch for cancer therapy has exquisite specificity for its allelic target antigen

Jee-Young Mock,[1,3] Aaron Winters,[1,3] Timothy P. Riley,[1] Richele Bruno,[1] Martin S. Naradikian,[1] Shruti Sharma,[1] Claudia A. Jette,[2] Ryan Elshimali,[1] Casey Gahrs,[1] Dora Toledo-Warshaviak,[1] Anthony P. West, Jr.,[2] Alexander Kamb,[1] and Agnes E. Hamburger[1]

[1]A2 Biotherapeutics, 30301 Agoura Road, Agoura Hills, CA 91301, USA; [2]Division of Biology and Biological Engineering, California Institute of Technology, Pasadena, CA 91125, USA

Innovative cell-based therapies are important new weapons in the fight against difficult-to-treat cancers. One promising strategy involves cell therapies equipped with multiple receptors to integrate signals from more than one antigen. We developed a specific embodiment of this approach called Tmod, a two-receptor system that combines activating and inhibitory inputs to distinguish between tumor and normal cells. The selectivity of Tmod is enforced by the inhibitory receptor (blocker) that recognizes an antigen, such as an HLA allele, whose expression is absent from tumors because of loss of heterozygosity. Although unwanted cross-reactivity of the blocker likely reduces efficacy rather than safety, it is important to verify the blocker's specificity. We have tested an A*02-directed blocker derived from the PA2.1 mouse antibody as a safety mechanism paired with a mesothelin-specific activating CAR in our Tmod construct. We solved the crystal structure of humanized PA2.1 Fab in complex with HLA-A*02 to determine its binding epitope, which was used to bioinformatically select specific class I HLA alleles to test the blocker's functional specificity *in vitro*. We found that this A*02-directed blocker is highly specific for its cognate antigen, with only one cross-reactive allele (A*69) capable of triggering comparable function.

INTRODUCTION

Engineered immune cells have emerged over the past decade as a promising therapeutic modality for cancer and other diseases.[1–3] However, cell therapy must still overcome a key obstacle in oncology: the scarcity of molecules that unequivocally differentiate tumor from normal tissues. Cell therapies have the potential to directly tackle this challenge because they can integrate multiple signals in complex cellular environments. This capability enables more sophisticated mechanisms to detect tumor cells. In principle, nuanced responses to distinct cellular antigen profiles may allow engineered cells to deliver selective cytotoxic blows, perhaps approaching the extraordinary precision of the adaptive immune system.[4]

One recently described synthetic circuit designed to integrate multiple signals is Tmod (A2 Biotherapeutics), a dual-receptor system that incorporates an activating chimeric antigen receptor (CAR) or T cell receptor (TCR) and an inhibitory component.[5–7] In one format, Tmod cells express an HLA-I-gated blocker that protects normal tissues while releasing the brake on cytotoxicity against cells that lack expression of HLA-A*02 (referred to as A*02 from this point on). Because a high percentage of tumors (~15%; https://www.cancer.gov/tcga)[8,9] retain only one HLA allele because of loss of heterozygosity (LOH), heterozygous A*02 patients with specific LOH in their tumors can be identified for treatment.[9,10] Such LOH irreversibly eliminates an allele such as A*02 that would otherwise protect the neoplastic cells from attack by Tmod cells. The Tmod system is flexible and modular, allowing a variety of activator receptors to be paired with the A*02 blocker. Furthermore, other HLA-I alleles can serve as the blocker antigen, readily extending the platform to patients beyond those with germline A*02.[7]

HLA-I is a surface protein expressed throughout the body, providing a broadly active safety input. HLA-I proteins also display sequence variation on the surface of their extracellular domains, allowing discrimination of one allelic product vs. another by a specific blocker, thus marking specific tumor cells for destruction. However, the extensive polymorphism of HLA alleles engenders a risk that binders may cross-react with related allelic products. Indeed, HLA is one of the most polymorphic loci known, with thousands of closely related alleles in the human population.[11] Therefore, it is important that a Tmod blocker component intended for the clinic be tested thoroughly to understand the limits of its specificity. Such data help inform decisions about which patients should be included and excluded from treatment, maximizing the chances for benefit in the population. Specifically, detailed information about blocker selectivity can identify A*02(+) patients who may not respond to the Tmod therapy because they express an HLA-I allele that cross-reacts with the A*02 blocker, impeding efficacy even in tumors that have been selected for A*02 loss.

Received 26 May 2022; accepted 30 September 2022;
https://doi.org/10.1016/j.omto.2022.09.010.

[3]These authors contributed equally

Correspondence: Alexander Kamb, PhD, A2 Biotherapeutics, 30301 Agoura Road, Agoura Hills, CA 91301, USA.
E-mail: akamb@a2biotherapeutics.com
Correspondence: Agnes E. Hamburger, A2 Biotherapeutics, 30301 Agoura Road, Agoura Hills, CA 91301, USA.
E-mail: ahamburger@a2biotherapeutics.com

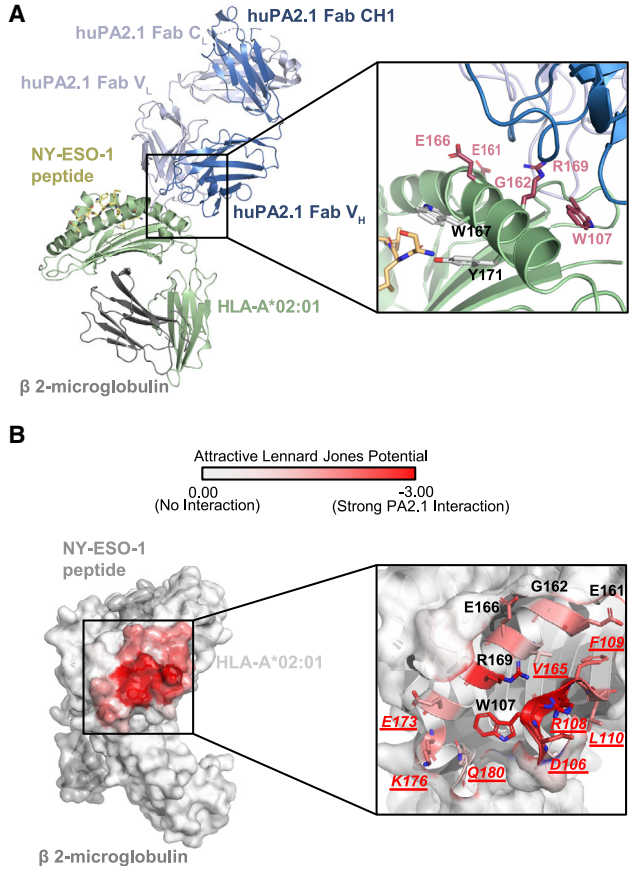

Figure 1. Crystal structure of the humanized PA2.1 Fab and A*02-NY-ESO-1(V) pMHC complex

(A) Structure of the humanized PA2.1 (huPA2.1) Fab/A*02-NY-ESO-1(V) pMHC complex in ribbon representation. Heavy chain and light chain of the Fab are shown in dark blue and light blue, respectively. HLA molecule is shown in green, and β_2-microglobulin shown in gray. Peptide is represented in yellow sticks. (Inset) The side chains of the 7 residues initially identified as the PA2.1 epitope are represented as sticks. The 5 residues that make direct contact with the Fab are highlighted in magenta. (B) Surface representation of the HLA-A*02-NY-ESO-1(V) complex at the PA2.1 interface (left). Interacting residues are highlighted in red relative to the strength of the Lennard Jones potential. The 13 A*02 residues that interact with PA2.1 are highlighted as red sticks on the right. Residues forming additional interactions with PA2.1 not predicted by Parham et al.[12] are underlined in red text.

Here we describe detailed analysis of an A*02-directed blocker module that is part of several therapeutics under consideration for clinical development.[6,7] This blocker has a ligand-binding domain (LBD) based on the PA2.1 monoclonal antibody (mAb) discovered more than 40 years ago and characterized by Parham and colleagues in subsequent years.[12,13] We solved the crystal structure of the PA2.1 Fab in complex with A*02:01 to identify the binding epitope of PA2.1 that was previously defined by a variety of biochemical, structural modeling, and comparative sequence studies.[12] We determined PA2.1 recognition is driven by a 13-residue epitope, with 2 key residues sufficiently differentiating HLA-A*02 from other alleles. A thorough functional analysis showed that, apart from the previously identified strongly cross-reacting A*69 allele, the A*02-directed blocker displays very high specificity for its cognate A*02 antigen in both primary T and Jurkat cells, with only weak cross-reactivity to two rare A*24 alleles. These findings support the choice of this blocker to explore the behavior of the Tmod system in clinical trials.

RESULTS

Binding assays confirm that PA2.1 mAb and scFv recognize A*02 and A*69 alleles

We first set out to confirm the published binding behavior of the PA2.1 mouse IgG (muIgG) LBD. Because we were ultimately interested in testing the sequence in a single-chain variable fragment (scFv) format, we converted the mouse mAb to its murine and humanized scFv equivalents (muscFv, huscFv; see materials and methods). The scFv was expressed with either a LIR-1 hinge or mutant monomeric CD8 hinge lacking cysteine residues and fused via its C terminus to a stabilized, monomeric human Fc (monoFc)[14] and purified from Expi-CHO-S cells (Figure S1A). These scFv-hinge-Fcs were used to confirm the binding profile of the LBD across 72 HLA-I antigens displayed in the FlowPRA Single Antigen kit (One Lambda) (Figure S1B). FlowPRA is a binding detection method based on HLA-I single antigen beads (SABs) analyzed using flow cytometry (Figure S1C). Similar bead-based kits were previously used to assess specificity of the PA2.1 mAb in the IgG format.[12] A positive pan-HLA-I mAb (W6/32) served as positive control and comparator; an irrelevant mesothelin (MSLN) directed scFv hinge-Fc served as negative control. At 5 μg/mL concentration, the muIgG, the muscFv, and the huscFv all showed selective binding to A*02 and A*69 alleles (Figure S1D), consistent with previous studies.[12] Weak, concentration-dependent binding was detected to other HLA-I alleles in both the IgG and scFv formats, also as previously seen.[12]

Crystal structure of PA2.1 Fab in complex with HLA-A*02

To fully define the molecular basis of PA2.1 specificity, we determined the co-crystal structure of the PA2.1 Fab with HLA-A*02 (Figure 1A; see also Table S1). The PA2.1 complementarity-determining regions (CDRs) were grafted onto a humanized Fab framework and purified as a complex with soluble A*02:01 bound to a modified NY-ESO-1-derived peptide MHC (A*02:01-NY-ESO-1[V] pMHC). The Fab-pMHC complex produced well-formed crystals and a complete dataset was collected and refined at 2.9 Å. Using the refined structures, atomic interactions were calculated within the Rosetta Protein Design Suite[15] and mapped onto the structure. As predicted by previous studies,[12] the Fab primarily interacts with residues on the α2 domain of the HLA molecule (Figure 1A). Of the 7 residues initially predicted, 5 (W107, G162, E161, E166, and R169) were confirmed to make direct interactions with PA2.1 (Figure 1A, residues highlighted in magenta). The structure revealed that the other 2 residues (W167 and Y171) previously predicted to be critical for PA2.1-A*02 interaction are not located at the binding interface and instead reside within the peptide-binding groove (Figure 1A). In addition to the amino acids previously identified,[12] the PA2.1 Fab forms additional van der Waals interactions with HLA-A*02 residues D106, R108, F109, L110, V165, E173, K176, and Q180 (Figure 1B). Most of the contacts

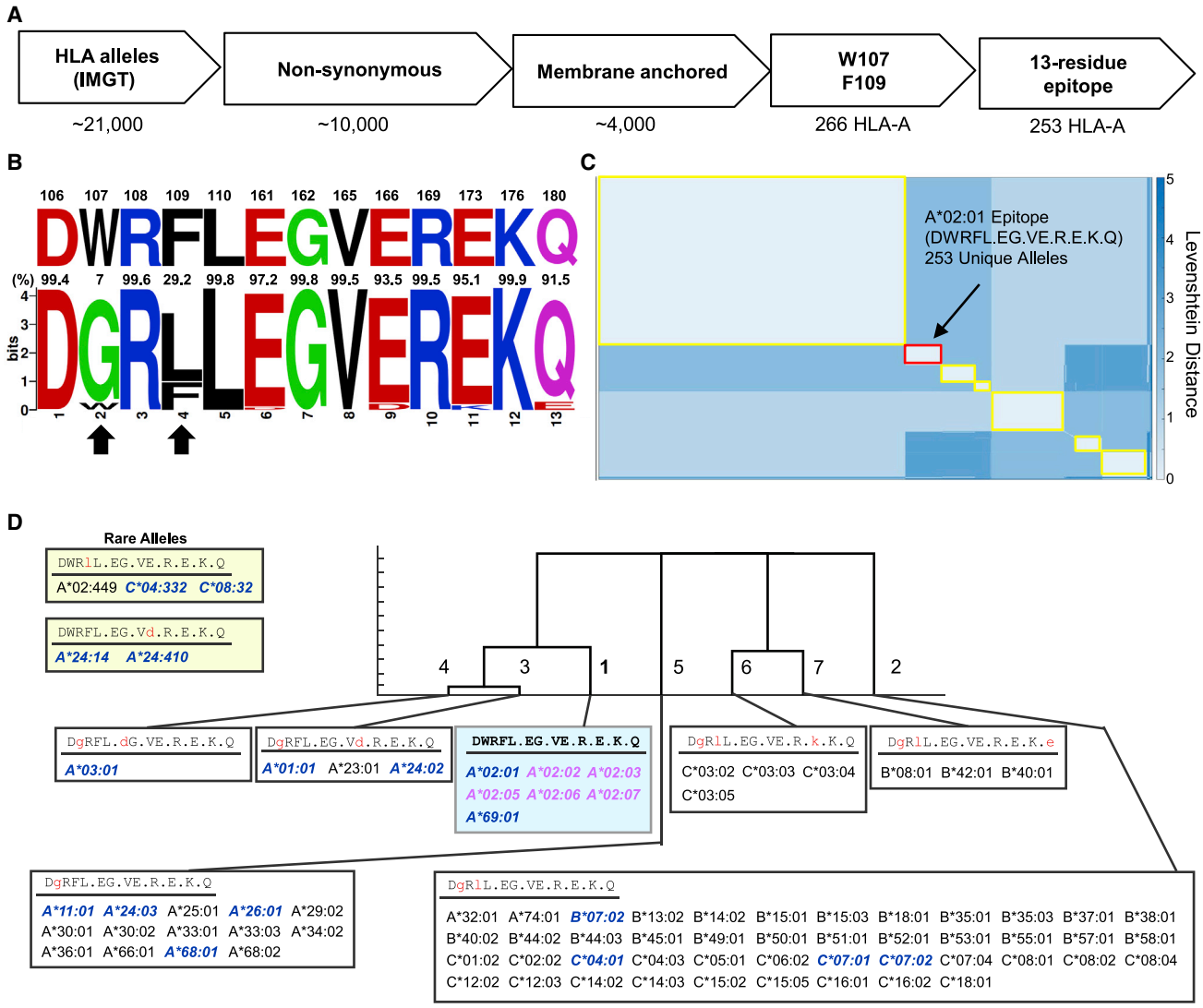

Figure 2. Allele classification on the basis of PA2.1 epitope similarity to A*02

(A) Schematic representation of the workflow used to identify HLA class I alleles most similar to HLA-A*02:01. (B) A sequence logo reveals the 13-residue PA2.1 epitope on HLA-A*02 (top) is highly conserved across membrane-bound HLA class I alleles (bottom). (C) Clustering the membrane-bound HLA class I alleles by Levenshtein distance identified 7 unique PA2.1 epitopes that constitute more than 96% of the HLA population. (D) A dendrogram highlights the relationships of the 7 distinct epitope clades. The 75 most frequent HLA-A, B, and C alleles are listed and categorized on the basis of epitope clade.

are mediated by CDRs 1, 2, and 3 of the heavy chain, with some contributions from CDR1 and 3 of the light chain (Figure S2).

Identification of potentially cross-reactive alleles on the basis of sequence similarity to A*02

Using the expanded epitope identified above, we next undertook a bioinformatics search to identify the key determinants of PA2.1 specificity. From the ~21,000 total HLA class I alleles in the international ImMunoGeneTics information system (IMGT),[16] we identified ~10,000 sequences with nonsynonymous substitutions. Excluding sequences without a predicted transmembrane domain (TM) left ~4,000 HLA-I homologs for analysis (Figure 2A). Sequence alignment revealed that the region comprising the 13-residue PA2.1 epitope is highly conserved, with most alleles sharing more than 90% epitope identity with HLA-A*02:01 (Figure 2B). Indeed, the sequence of HLA-A*02:01 differed significantly from the consensus at only two positions: W107, previously identified as a key contributor to PA2.1 recognition,[12] and F109, implicated only through the structure described in this study (Figure 2B, highlighted in arrows).

Further analysis of the major alleles revealed 96.1% of investigated class I alleles clustered into 7 epitope clades, with only one clade (encompassing HLA-A*02:01) sharing both W107 and F109 (Figure 2C). Structural models of the PA2.1 interaction with each of these seven

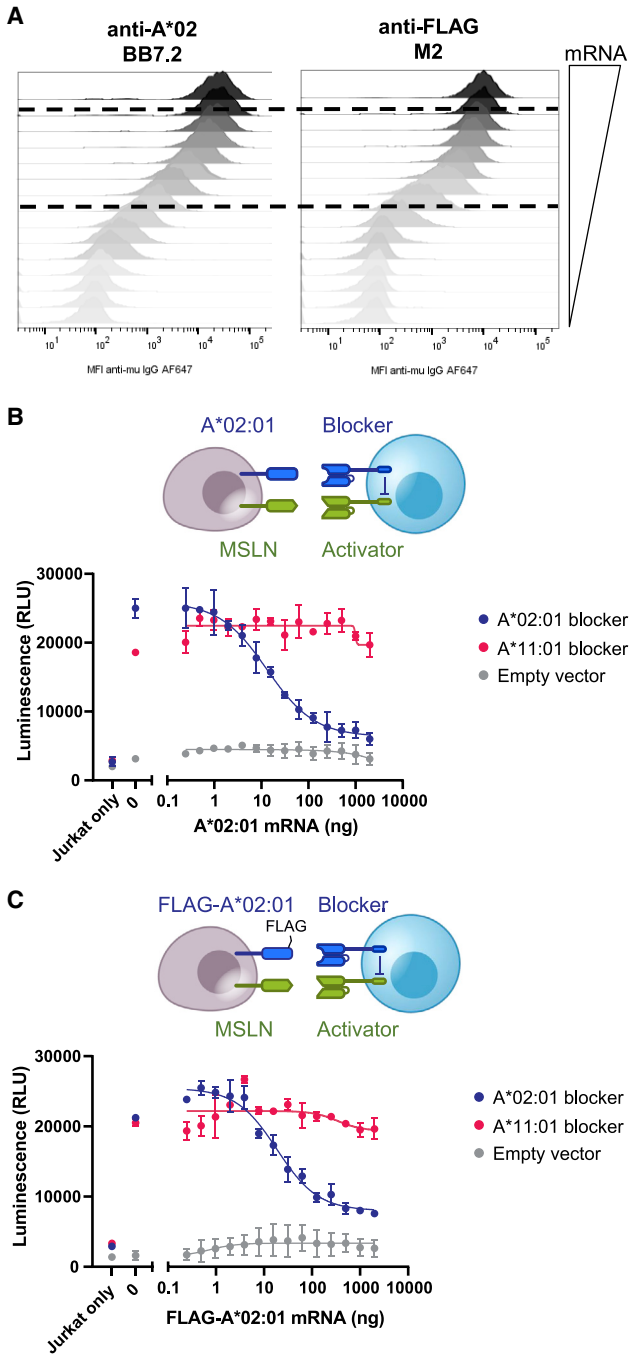

Figure 3. FLAG-tagged HLA-I constructs fold and function properly

(A) Titration of 2 μg FLAG-tagged HLA-A*02:01 mRNA 2-fold across 15 points results in varied amounts of HLA-A*02:01 on the surface of HeLa cells. FLAG-tagged HLA-A*02:01 detected with anti-HLA-A*02 mAb (BB7.2) or anti-FLAG mAb (clone M2). Dashed black lines indicate the relative expression range of HLA A*02 observed on normal cells. (B) Jurkat-NFAT luciferase assay with untagged HLA-A*02:01 titration. Jurkat effector cells expressing both MSLN CAR combined with either PA2.1 A*02 blocker, irrelevant A*11 blocker, or empty vector (blue cell cartoon) were co-cultured with HeLa target cells with titrating amounts of untagged A*02:01 mRNA (purple cell cartoon). (C) Jurkat-NFAT luciferase assay with N-terminally FLAG-tagged HLA-A*02:01 titration. Jurkat effector cells are represented in the blue cartoon, while HeLa target cells are represented in purple. Co-culture assay was performed as described in (B). Data shown for (B) and (C) depict mean +/- SD from 2 technical replicates.

clades revealed that computationally generated changes to either W107 or F109 resulted in substantial increases in predicted free energy of the complex (Table S2). Although Rosetta energy units are arbitrary and relative, higher scores often translate to weaker affinities[17] and thus provide a structural rationale for the PA2.1 specificity observed. Indeed, only the clade containing the unmodified 13-residue HLA-A*02:01 epitope did not negatively affect predicted binding affinity (Table S2). This clade consisted of 253 unique HLA alleles (Figure 2A), which mostly encompassed HLA-A*02 alleles, except for three HLA-A*69 variants. Next, we individually examined the sequences of the remaining 3.9% (149 total) unclustered alleles and identified 20 additional alleles that differed from the HLA-A*02:01 epitope sequence by a single residue. Thirteen of these alleles shared both W107 and F109, with 11 comprising HLA-A*02 alleles and two rare HLA-A*24 alleles (A*24:14 and A*24:410; population frequency < 1e-5). Three alleles did not contain W107 (A*02:784, A*11:206, and A*26:39) and the remaining four alleles (A*02:449, A*02:661, C*04:332, and C*08:32) did not contain F109 but were otherwise identical to the HLA-A*02:01 epitope sequence.

Identification of high-frequency alleles and selective functional inhibition by the A*02 blocker in primary T cell cytotoxicity assays

To investigate the significance of the individual epitope clusters, we mapped the epitopes of the most frequent alleles in the human population. As expected, the top 25 most frequent HLA-A, B, and C alleles represented all 7 of the major epitope clades, with 5 common HLA-A*02 alleles sharing the full HLA-A*02:01 epitope sequence (Figure 2D). Coincidentally, this analysis included many of the common alleles evaluated in the binding studies above (Figure S1), which further validated the selectivity of PA2.1 for the HLA-A*02:01 epitope clade. However, as binding does not fully predict function for TCRs, CARs, and their inhibitory receptor counterparts (see below[18,19]), we selected a set of 15 alleles for functional analysis. We prioritized alleles on the basis of number of mismatched epitope residues as well as frequency of occurrence. We also considered alleles of lower population frequency with $\leq$1 mismatched residue to capture alleles with high sequence similarity to HLA-A*02. The selected 15 alleles encompassed high-frequency alleles from 5 of the 7 epitope clades with high similarity to HLA-A*02:01, in addition to a lower frequency A*69 allele that shares the full epitope and two rare HLA-C alleles that differ from HLA-A*02:01 only at the newly identified F109 position (Figure 2D, highlighted in blue italics).

To create constructs whose expression and function in cells could be monitored easily, we designed and synthesized mRNA encoding N-terminally FLAG-tagged HLA-I antigens of interest. Surface expression of one of these representative HLA molecules, A*02:01,

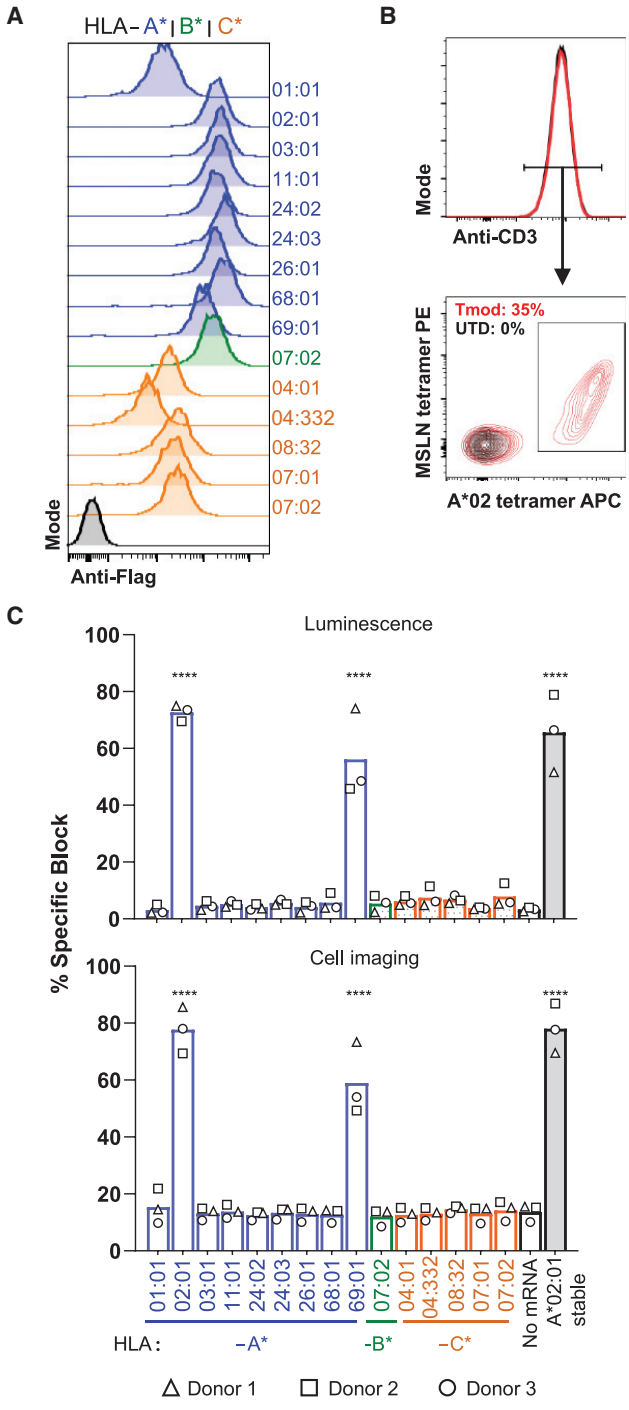

Figure 4. Primary Tmod cytotoxicity assay confirms PA2.1 allele specificity

(A) FACS histograms show surface expression of the specific FLAG-HLA alleles on the surface of HeLa cell 48 h post-transfection using anti-FLAG (DYKDDDDK) mAb. (B) Representative FACS plots showing CD3(+) untransduced (UTD, black) and Tmod transduced (red) T cells' capacity to bind biotinylated MSLN tetramer-PE and HLA-A*02:01 tetramerized with streptavidin-APC. (C) Percentage HLA allele-specific blocking by Tmod cells after 48 h of co-culture with transfected GFP+ *Renilla* luciferase(+) HeLa cells on the basis of terminal luminescence measurements (top panel) and live cell imaging from Incucyte (bottom panel). Data shown for (C) depict the average of 3 individual HLA A*02(−) donors analyzed using an ordinary one-way ANOVA with Bonferroni's multiple-comparisons test relative to "no mRNA." ****$p < 0.0001$; all other comparisons were not significant. Functional behavior of these Tmod constructs in HLA A*02 (+) T cells can be found in Tokatlian et al. (2022).[7]

could be detected using both anti-A*02 and anti-FLAG antibodies (Figure 3A). Importantly, mRNA transfected HeLa cells expressed A*02 surface protein comparably to normal human tissue as previously reported.[7] To characterize the effect of the N-terminal FLAG-tag on surface expression and recognition by PA2.1-derived receptors, we titrated synthetic mRNA encoding the HLA-I heavy chain with or without N-terminal FLAG-tag in A*02(−) HeLa cells. When these HeLa cells were mixed with Jurkat effector cells that expressed an MSLN CAR ± the A*02 blocker, dose-response curves were generated consistent with the proper folding and function of the untagged (Figure 3B) and FLAG-tagged A*02:01 molecules (Figure 3C).

With these reagents in hand, we proceeded to test A*02 blocker selectivity in primary T cells. Of the 15 alleles selected for investigation, all but one of the rare C alleles expressed well (Figure 4A). MSLN Tmod cells generated from three donors (Figure 4B) were co-cultured with MSLN(+) GFP and *Renilla* luciferase-expressing HeLa cells transfected with different FLAG-tagged HLA-I heavy chain mRNAs (Figure 4A). Only clade I members A*02 and A*69, which contain the full 13-residue epitope, including both critical aromatic residues W107 and F109, triggered blocking function when the target cells expressed the HLA-I antigen, revealed by the presence of viable transfected HeLa cells in the co-culture 48 h after incubation (Figure 4C).

Selective activation and inhibition mediated by the PA2.1 scFv in Jurkat cell reporter assays

Because primary T cell cytotoxicity is the most direct therapeutically relevant readout, these data strongly support the functional specificity of the A*02-directed blocker. However, given the complexity of primary T cell assays, further exploration of the specificity in the context of other conventional assays was deemed worthwhile. We thus tested additional functions of the A*02 blocker in Jurkat cell assays. In the first case, we explored the ability of these alleles to block MSLN CAR function in Jurkat cells that co-expressed the blocker. These experiments were conducted in a similar fashion as the primary T cell assays except that NFAT-reporter-engineered Jurkat cells were used as effector cells.[20] Comparisons of MSLN(+) HeLa target cells with or without expression of the HLA-I allele demonstrated that A*02 and A*69 blocked activation robustly (Figure 5A; see also Figures S3A and S3B). Additionally, the rare A*24 alleles containing 12 of 13 epitope residues weakly cross-reacted with PA2.1, confirming that although W107 and F109 are most critical for the interaction, all 13 residues contribute to the functional response of the receptor.

Encouraged by these data that extended the findings in primary T cells to another cell type (Jurkat), we tested an even simpler format

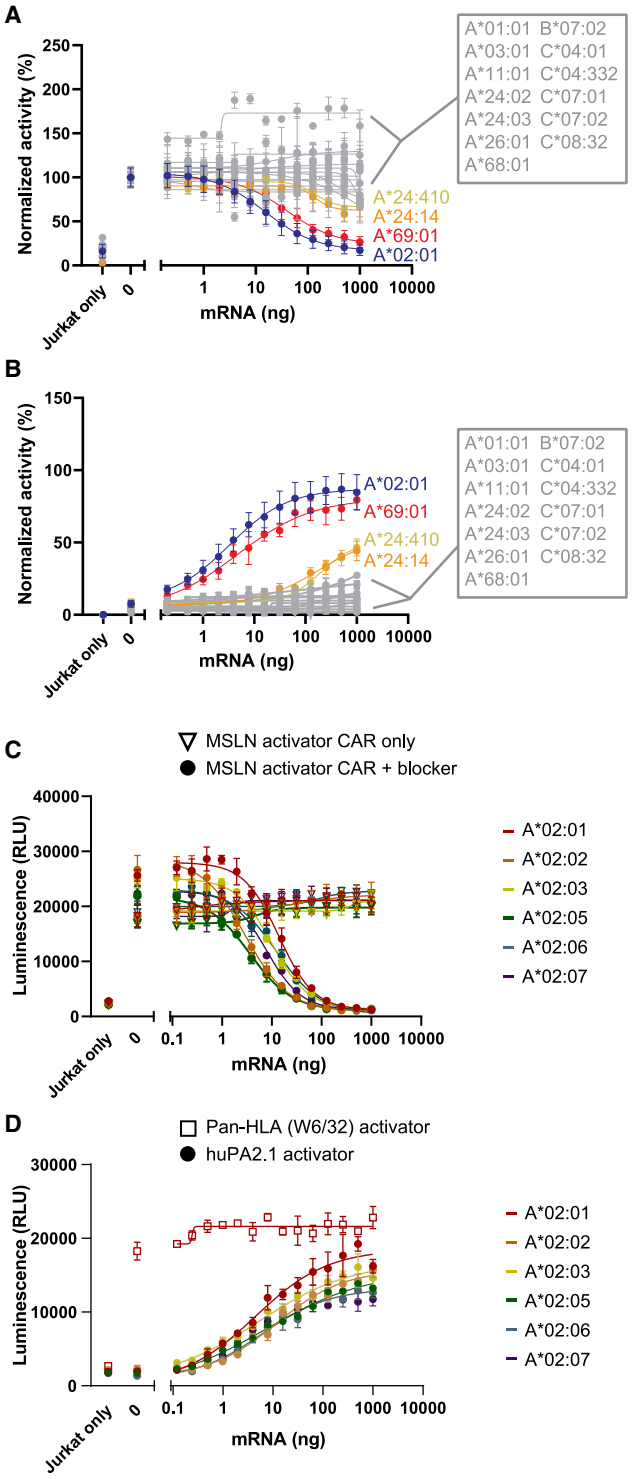

Figure 5. Jurkat-NFAT luciferase response using either blocking or activating receptor is predictive of immune receptor function in T cells

(A) Jurkat-NFAT luciferase functional assay to measure huPA2.1-derived A*02 blocker activity against 15 bioinformatically identified alleles. MSLN CAR was paired with huPA2.1-derived A*02 blocker. FLAG-tagged HLA mRNA was titrated in HeLa cells. Jurkat cell responses to FLAG-A*02:01 and FLAG-A*69:01 mRNA are highlighted in blue and red, respectively. To account for run-to-run variation, NFAT response was normalized, for which 100% NFAT response is equivalent to NFAT response when 0 ng of HLA mRNA is transfected for each construct. (B) Jurkat-NFAT luciferase functional assay to measure PA2.1 scFv CAR-derived A*02 activator function against 15 bioinformatically identified alleles. FLAG-tagged HLA mRNA was titrated in HeLa cells. Jurkat cell responses to FLAG-A*02:01 and FLAG-A*69:01 mRNA are highlighted in blue and red, respectively. To account for run-to-run variation, data were normalized by grouping constructs that were characterized on the same replicate together. For each replicate, the highest NFAT luciferase response of A*02:01 activation was considered the maximum signal. All NFAT signals for other constructs were divided by this maximum signal and plotted as percent of maximum A*02:01 NFAT signal. (C) Jurkat-NFAT luciferase functional assay to measure huPA2.1-derived A*02 blocker activity against additional HLA-A*02 alleles. huPA2.1 blocker was paired with MSLN CAR. (D) Jurkat-NFAT luciferase functional assay to measure huPA2.1-derived A*02 activator activity against additional HLA-A*02 alleles. A pan-HLA-I activator CAR with an scFv derived from W6/32 mAb[21] was used as a positive control. Data from C) and D) depict mean +/- SD of 3 technical replicates.

for detection of off-target functional activity of PA2.1 scFvs. In this case, we constructed a third-generation activating CAR (CD28-41BB-CD3ζ) that incorporated the PA2.1 scFv as the LBD. As expected, only the alleles containing both critical epitope residues, W107 and F109, produced activation signal. Furthermore, only the two alleles with all 13 epitope residues, A*02 and A*69, elicited substantial activation of Jurkat cells, suggesting that the specificity of the LBD observed in the blocker format is retained in the activator format (Figure 5B; see also Figures S3C and S3D).

As a final step in the characterization of the PA2.1 scFv, we used the Jurkat assays to confirm that the scFv has pan-A*02 specificity. We tested the next 5 most frequent A*02 alleles in clade I (Figure 2D, highlighted in pink italics), A*02:02, A*02:03, A*02:05, A*02:06, and A*02:07, and showed the expected function in both the blocker (Figure 5C) and activator (Figure 5D) formats. These results confirm that the epitope revealed by the crystal structure is predictive of function of PA2.1-derived chimeric immune receptors.

DISCUSSION

The Tmod system combines two receptors to enforce specificity of response: an activator and a blocker. Tmod constructs and their individual components can be tested for off-target behavior in highly sensitive functional assays.[19] Such assays are preferable to simple binding studies because of the well-known disconnect between binding and function for TCRs and CARs.[18,19,22] Tmod cells are expected to respond specifically to target antigens because their activation is initiated by receptors that are often highly optimized TCRs or CARs derived from mAbs. Adding to this level of specificity, the Tmod constructs studied here include an inhibitory receptor that targets a blocker ligand (A*02) ubiquitously expressed on nucleated cells that should tamp down any CAR or TCR activation stimulus. Indeed, Tmod constructs have been shown to exhibit minimal activation in the presence of activating stimuli derived from

either CARs or TCRs, so long as the blocker antigen is present on the target cells.[5–7,19]

Unwanted inhibition caused by expression of closely related HLA-I alleles is the focus of this paper. We have systematically surveyed a large number of HLA-I alleles and concentrated on those most likely to cross-react with the A*02-directed blocker module of interest. Such cross-reactivity, if unaccounted for, would be expected to blunt the efficacy of Tmod treatment in patients who carry the cross-reacting alleles. If cross-reactivities were known, patients with corresponding haplotypes could be excluded from treatment by an appropriate diagnostic test. However, such exclusions limit the breadth of application of the therapy and would be especially problematic if the excluded alleles were frequent thereby decreasing the eligible patient population. Here we focused on the frequent HLA-I alleles because they are most likely to be encountered in a clinical context. To extend these results even more broadly, it will ultimately be useful to develop predictive models based solely on primary sequence. Structure-function studies of CARs have shown that the specificity and sensitivity tracks mainly with the LBD.[18,23] Our results with the A*02 blocker suggest that this feature also applies to inhibitory receptors. As the Tmod approach is extended beyond the A*02-directed blocker to blockers that target other HLA alleles, it will be critical to develop evidence similar to that reported here which support specificity of function in the context of the highly variable HLA genotypes that exist in the patient population. On the basis of the overall consistency of the results presented here, we believe it may ultimately be possible to test cross-reactivity of other blockers (i.e., beyond the PA2.1-based blocker) using the simpler format of Jurkat cell assays. Alleles that display cross-reactivity above a certain threshold can then be excluded from treatment because of the possibility that they may limit efficacy.

To investigate potential cross-reactivity, we have taken advantage of the enormous datasets collected over decades of HLA study. The central importance of HLA genes to immune function, and graft rejection in particular, has triggered massive investment in the collection of detailed population-based information. In addition, HLA allelic products were among the first targets studied with mAbs in the 1970s.[21] The utility and specificity of these mAbs reflect the diligence of early investigators who discovered and characterized them. The sensitive binding and functional assays used here confirmed the previously known reactivity of the PA2.1 LBD to both A*02 and A*69,[12] and uncovered weak cross-reactivity to A*24:14 and A*24:410. Although it is tempting to conclude from this experience that binding studies may be sufficient, collective experience in this field suggests that functional assays combined with sequence-based analysis are vital to ensure the most potent, individualized treatment for patients.[18,22]

MATERIALS AND METHODS

Construct design and cloning

PA2.1 humanization was carried out by grafting mouse CDRs onto frameworks of human antibody sequences with close sequence identity to the mouse framework. scFvs were then designed using flexible (G4S)3 linker to connect the VH and VL domains. All soluble scFvs were fused to either CD8α hinge (residues 138–182) with disulfide cysteines mutated to serine, or LILRB1 (LIR-1) hinge (residues 398–461), followed by previously described C-terminal monomeric Fc.[14] All third-generation activator CAR constructs contained CD8 hinge fused to CD28 TM, as well as CD28, 4-1BB, and CD3z intracellular domains (ICDs). All blocker receptor constructs contained LILRB1 hinge, TM, and ICD. Template used for N-terminally FLAG-tagged HLA mRNA synthesis contained 5′ T7 promoter followed by the V kappa 1 signal peptide, 1× FLAG peptide (DYKDDDDK), and G4S linker. All DNA constructs were assembled using Golden Gate Assembly. DNA templates were either amplified by PCR or linearized by restriction enzyme digest, then mRNA was synthesized using the HiScribe T7 ARCA mRNA kit (New England Biolabs). The *in vitro* synthesized mRNA was purified using the Monarch RNA Cleanup Kit (New England Biolabs), eluted in 1 mM sodium acetate, and stored at −80°C.

muPA2.1 IgG and scFv expression and purification for binding studies

The muPA2.1 IgG was generated via hybridoma culture (American Type Culture Collection [ATCC] HB-117) followed by protein G immunoaffinity purification. DNA plasmid encoding the PA2.1-derived scFv-Fc was transfected into Expi-CHO-S cells (Thermo Fisher Scientific) using the ExpiFectamine CHO Transfection kit per manufacturer's instructions (Thermo Fisher Scientific). During the 7–10 days of expression, cell viability was monitored, and conditioned medium was harvested at 10 days or if cell viability dipped below 80%. The conditioned medium was diluted 1:1 with Pierce Protein A/G IgG Binding Buffer (Thermo Fisher Scientific). Pierce Protein A/G Plus Agarose resin (1 mL) was carefully loaded onto gravity purification column and equilibrated with Pierce Protein A/G IgG Binding Buffer. The 1:1 diluted conditioned medium was loaded onto equilibrated resin. The resin was washed 1× with 10 mL of Pierce Protein A/G IgG Binding Buffer. Bound and washed scFv-Fc fusion molecules were eluted with 9 mL Pierce IgG Elution Buffer (Thermo Fisher Scientific) supplemented with 1 mL of 1 M Tris-HCl (pH 8.0) for pH neutralization. The resulting proteins were concentrated and loaded onto Superdex Increase 200 chromatography column (Cytiva) using gel filtration buffer, 20 mM Tris (pH 8.0), and 150 mM NaCl. Fractions were pooled, concentrated, and flash frozen in liquid nitrogen until use.

FlowPRA binding screens

FlowPRA Single Antigen beads (One Lambda) displaying 72 HLA class 1 alleles were washed and arrayed into 96-well microtiter plates. Twenty-five and 5 μg/mL concentrations of either mouse IgG or scFv-Fc fusion proteins were prepared via dilution into 1× FlowPRA dilution buffer (One Lambda). The mouse IgG and fusion proteins were incubated with each group of FlowPRA beads for 1 h, followed by 3 complete washes with FlowPRA dilution buffer (One Lambda). The bead + scFv-Fc complexes were incubated with a goat anti-human IgG, Fc-specific APC secondary antibody (The Jackson Laboratory), while mouse IgG bead complexes were incubated with a goat anti-mouse IgG, Fc APC secondary antibody (The Jackson Laboratory).

After 30 min, the bead sets were again washed 3 times and resuspended in wash buffer, and data were acquired on a BD FACS Canto flow cytometer running Diva software. FCS files were analyzed using FlowJo software to quantify allele-specific MFI values.

Fab and pMHC expression and purification for crystallization

For Fab production, Expi-CHO-S cells were transfected and conditioned medium harvested as described above. Harvested conditioned medium was loaded directly onto 5 mL CaptureSelect CH1-XL prepacked column (Thermo Fisher Scientific) using loading buffer 10 mM Tris-HCl (pH 8.0), 100 mM NaCl. Column was washed with 10 column volumes of loading buffer. Fab was eluted using 5 column volumes of 50 mM acetate (pH 5.0) buffer directly into tubes containing 1 M Tris-HCl (pH 8.0), bringing the final concentration of Tris-HCl (pH 8.0) in the fractions to 100 mM. Fractions containing Fab were pooled, concentrated, and loaded onto Superdex Increase 200 column using crystallization gel filtration buffer (20 mM Tris [pH 8.0], 50 mM NaCl). Correctly folded fraction was pooled and concentrated.

HLA-A*02-NY-ESO-1(V) peptide MHC complex was expressed and purified as described previously with modifications.[18] Briefly, HLA-A*02:01 and human β-2 microglobulin were expressed in One Shot BL21(DE3)pLysS (Invitrogen) cells. Cells were lysed and inclusion body was isolated and washed. Inclusion body was solubilized in 25 mM MES (pH 6.0), 8 M urea, and 10 mM EDTA. Insoluble fraction was removed by centrifuging at 10,000 × *g* for 20 min at 4°C. Urea-solubilized protein was flash frozen in liquid nitrogen until use. HLA-A*02:01, human β-2 microglobulin, and a modified NY-ESO-1(V) peptide (SLLMWITQV; with a valine [V] substituted for the C-terminal cysteine) was refolded in 100 mM Tris-HCl (pH 8.0), 500 mM L-arginine, 2 mM EDTA, 5 mM reduced glutathione, 0.5 mM oxidized glutathione, and 1× protease inhibitor cocktail (Thermo Fisher Scientific) at 10°C while stirring. After 48–72 h, resultant refolding reaction was filtered using 0.4 μM vacuum filtration device and concentrated using Amicon centrifugal concentrators (Millipore). The protein sample was desalted using the PD-10 Desalting Column (Cytiva) to 20 mM Tris-HCl (pH 8.0). The buffer exchanged sample was loaded onto HiTrap CaptoQ ImpRes anion-exchange chromatography column (Cytiva), with salt gradient from 0 to 150 mM NaCl (20 mM Tris-HCl [pH 8.0]). Fractions containing pMHC probe was confirmed by SDS-PAGE Coomassie staining. Fractions were pooled, concentrated, and loaded onto Superdex Increase 200 column (Cytiva) with final gel filtration buffer 20 mM Tris-HCl (pH 8.0), 50 mM NaCl.

Crystal structure of huPA2.1 Fab/A*02-NY-ESO-1(V)

To generate crystallization-grade huPA2.1 Fab/A*02-NY-ESO-1(V) complex, Fab and A*02-NY-ESO-1(V) pMHC purified above were co-incubated at a 1:1 or 1:10 ratio. The resulting complex was loaded onto Superdex Increase 200 column (Cytiva), and fractions running at higher molecular weight was confirmed to be Fab-A*02-NY-ESO-1(V) complex by SDS-PAGE. The complex fraction was pooled and concentrated to ∼8 mg/mL and left at 4°C for ∼4 days. Prior to crystallization trial, the concentrated protein sample was centrifuged at ∼18,000 × *g* at 4°C for 10 min to remove any precipitants.

Crystallization trials with commercial screens (Hampton Research) were performed at room temperature using the sitting drop vapor diffusion method by mixing equal volumes of Fab-pMHC complex and reservoir using a TTP LabTech Mosquito robot. Initial crystal hits were optimized manually in large-format grease trays. Fab-pMHC crystals obtained in 0.2 M L-Proline, 0.1 M HEPES (pH 7.5), 13% PEG3350 were cryoprotected in a mixture of well solution with 20% glycerol and then frozen in liquid nitrogen.

X-ray diffraction data were collected for Fab-pMHC crystals at the Stanford Synchrotron Radiation Lightsource (SSRL) beamline 12-2 on a Pilatus 16 M pixel detector (Dectris) at a wavelength of 0.98 Å. Data from a single crystal in the $P2_12_12_1$ space group were indexed, integrated, and scaled using XDS[24] and merged using AIMLESS version 0.7.4 in *CCP4* version 7.0.6[25] (Table S1). The structure was determined by molecular replacement with PHASER[26] using the coordinates for HLA-A2 with NY-ESO-1 peptide analog (PDB: 1S9X) and BHA10 Fab (PDB: 3HC0) after trimming heavy and light chain variable domains using Sculptor[27] as search models. Refinement of coordinates was performed using Phenix version 1.19.1[28] and cycles of manual building in Coot[29] (Table S1).

The atomic model generated from the X-ray crystallographic study of the PA2.1 Fab-HLA-A*02:01-NY-ESO-1(V) structure has been deposited at the Protein Data Bank (PDB) under accession code 8EB2.

Molecular modeling

Structural modeling and analysis of the PA2.1/pMHC interaction was performed using PyRosetta and the ref2015 score function.[30] Significant interactions between PA2.1 and HLA-A*02:01 were ranked according to scored energies and used to assemble the complete PA2.1 epitope. For modeling individual clades, the initial atomic coordinates were brought to a local energy minimum through five cycles of backbone minimization and rotamer optimization using the fastrelax protocol. For each epitope clade, mutations were computationally introduced onto the HLA-A*02 scaffold. This was followed by 50 Monte Carlo-based simulated annealing steps for the polypeptide backbone and surrounding residues. The final models were ranked relative to the relaxed starting model using the ref2015 score function.

HeLa cell transfections and HLA expression

Wild-type (WT) HeLa cells were cultured in fetal bovine serum (FBS) containing MEM media (Gibco) to approximately 80% confluency in T-225 flasks. On the day of transfection, the cells were lifted from the flasks using TryplyE express (Gibco), counted, and resuspended to 1.1e7 vc/mL. Select FLAG-tagged HLA mRNA was serially diluted 2-fold across 15 points in SE transfection buffer (Lonza) in 96-well v-bottom plates. WT HeLa cells were added to each well containing the mRNA at a concentration of 1.33e7 vc/mL. The mRNA/cell mixture was transferred to a 16-well Lonza 4D cuvette and

electroporated according to the manufacturer's protocol established for HeLa cells. Post-transfection, the cells were immediately placed into serum containing MEM growth media and seeded into rows of 384-well culture plates at a density of 2,500–5,000 cells/well, depending on experiment. Remaining transfected HeLa cells were seeded into separate 96-well plates specifically for fluorescence-activated cell sorting (FACS) expression testing. Plates were cultured for 18 h at 37°C and 5% CO_2.

Primary T cell cytotoxicity assay

Primary human T cells (Hemacare) from three HLA-A*02:01(−) donors depleted of CD56(+) cells and enriched on CD4 and CD8 (Miltenyi) were transduced with lentivirus (Lentigen) encoding the MSLN Gen3 CAR and PA2.1 blocker from a bicistronic vector at an MOI of 40. Cells were grown in GREX (Wilson Wolf) according to the manufacturer's instructions in X-VIVO 15 (Lonza, no phenol red) supplemented with 1% human serum (CELLect) and 300 IU/mL IL-2 (StemCell). Cytotoxicity assay was conducted as previously described[7] with the following modifications: *Renilla* luciferase(+) GFP(+) (rLuc GFP, Biosettia) HeLa target cells were used to enable Incucyte visualization and terminal luminescence measurements. RLuc GFP HeLa cells were transfected with 500 ng of various FLAG-HLA allele mRNA as described above, and 2,500 transfected target cells were allowed to settle overnight in 384-well plates. RLuc GFP HeLa targets were co-cultured with 1,250 Tmod or untransduced T cells for an effective E:T of 1:2 the following day for 48 h. All conditions were performed in triplicate in X-VIVO 15 media supplemented with 1% human serum without phenol or cytokine. Using *Renilla* luciferase substrate (Promega), relative luminescence values were captured (Tecan), and percentage specific blocking was calculated using the following formula:

$$100 - 100 \times [(A_{UTD} - A_{TD}) / A_{UTD}],$$

where L is raw luminescence value, UTD is untransduced, and TD is Tmod transduced T cell conditions. Incucyte software was used to calculate GFP(+) surface area between conditions. Percentage specific blocking was calculated using total GFP(+) surface area at 48 h with the following formula:

$$100 - 100 \times [(L_{UTD} - L_{TD}) / L_{UTD}],$$

where A is GFP+ surface area.

Jurkat-NFAT luciferase:HeLa cell co-culture assays

Jurkat-NFAT luciferase cells were cultured in FBS containing RPMI growth media to 1.5e6 vc/mL. Lentiviral constructs (Lentigen) were used at MOI of 5–10 to transduce Jurkat-NFAT luciferase cells with appropriate activator and blocker CARs and generate stable expressing activator and/or blocker expressing effector cells. Alternatively, Jurkat-NFAT luciferase cells were counted and 2e6 viable cells were resuspended in 120 µl of R2 buffer (Thermo Fisher Scientific) containing 2 µg DNA encoding the appropriate activator or blocker receptor construct. Immediately after transfection, cells were cultured overnight at 37°C 5% CO_2 in RPMI containing 20% FBS for co-culture assays the following day. Five thousand activating and/or blocker receptor expressing Jurkat-NFAT luciferase cells were combined with 5,000 HeLa HLA-I transfected target cells as described above in triplicate wells of a 96-well plate. The co-culture plates were incubated at 37°C, 5% CO_2 for 6 h. Fifteen microliters per well of luciferase substrate (BPS Biosciences) was added to each well of the plate. The plate was then incubated at room temp for 15 min and read on a Tecan M1000 luminescent plate reader with 100 ms integration time/well.

DATA AVAILABILITY STATEMENT

Raw data will be made available upon reasonable request.

SUPPLEMENTAL INFORMATION

Supplemental information can be found online at https://doi.org/10.1016/j.omto.2022.09.010.

ACKNOWLEDGMENTS

We thank Dr. Peter Parham for identifying and characterizing the original mouse anti-HLA A*02 antibody PA2.1, Dr. Pamela J. Bjorkman for supporting this work, Mark Daris for molecular biology and construct strategy, Kiran Deshmukh and Dr. Breanna DiAndreth for assistance with Jurkat cell assays, and Dr. Talar Tokatlian for helpful discussions and comments on the manuscript. Tmod is a trademark of A2 Biotherapeutics, Inc.

AUTHOR CONTRIBUTIONS

A.E.H. and A.K. conceived and designed the study. J.-Y.M., A.W., T.P.R., R.B., M.S.N., S.S., C.A.J., R.E., C.G., D.T.-W., and A.P.W. conducted experiments and/or analyzed data. A.K., A.E.H., J.Y.M., and A.W. wrote the manuscript. A.E.H. and A.K. supervised the project.

DECLARATION OF INTERESTS

A.E.H., A.K., J.-Y.M., A.W., T.P.R., R.B., M.S.N., S.S., C.J., R.E., C.G., and D.T.-W. are current or former employees and shareholders of A2 Biotherapeutics, Inc.

REFERENCES

1. Guedan, S., Ruella, M., and June, C.H. (2019). Emerging cellular therapies for cancer. Annu. Rev. Immunol. *37*, 145–171. https://doi.org/10.1146/annurev-immunol-042718-041407.

2. Melenhorst, J.J., Chen, G.M., Wang, M., Porter, D.L., Chen, C., Collins, M.A., Gao, P., Bandyopadhyay, S., Sun, H., Zhao, Z., et al. (2022). Decade-long leukaemia remissions with persistence of CD4(+) CAR T cells. Nature *602*, 503–509. https://doi.org/10.1038/s41586-021-04390-6.

3. Boardman, D.A., and Levings, M.K. (2022). Emerging strategies for treating autoimmune disorders with genetically modified Treg cells. J. Allergy Clin. Immunol. *149*, 1–11. https://doi.org/10.1016/j.jaci.2021.11.007.

4. Vivier, E., and Malissen, B. (2005). Innate and adaptive immunity: specificities and signaling hierarchies revisited. Nat. Immunol. *6*, 17–21. https://doi.org/10.1038/ni1153.

5. Hamburger, A.E., DiAndreth, B., Cui, J., Daris, M.E., Munguia, M.L., Deshmukh, K., Mock, J.Y., Asuelime, G.E., Lim, E.D., Kreke, M.R., et al. (2020). Engineered T cells directed at tumors with defined allelic loss. Mol. Immunol. *128*, 298–310. https://doi.org/10.1016/j.molimm.2020.09.012.

6. Sandberg, M.L., Wang, X., Martin, A.D., Nampe, D.P., Gabrelow, G.B., Li, C.Z., McElvain, M.E., Lee, W.H., Shafaattalab, S., Martire, S., et al. (2022). A carcinoembryonic antigen-specific cell therapy selectively targets tumor cells with HLA loss of heterozygosity in vitro and in vivo. Sci. Transl. Med. *14*, eabm0306. https://doi.org/10.1126/scitranslmed.abm0306.

7. Tokatlian, T., Asuelime, G.E., Mock, J.Y., DiAndreth, B., Sharma, S., Toledo Warshaviak, D., Daris, M.E., Bolanos, K., Luna, B.L., Naradikian, M.S., et al. (2022). Mesothelin-specific CAR-T cell therapy that incorporates an HLA-gated safety mechanism selectively kills tumor cells. J. Immunother. Cancer *10*, e003826. https://doi.org/10.1136/jitc-2021-003826.

8. McGranahan, N., and Swanton, C. (2017). Clonal heterogeneity and tumor evolution: past, present, and the future. Cell *168*, 613–628. https://doi.org/10.1016/j.cell.2017.01.018.

9. Jason Perera, B.M., Lau, D., Salahudeen, A., and Khan, A. (2019). Detection of Human Leukocyte Antigen Class I Loss of Heterozygosity in Solid Tumor Types by Next-Generation DNA Sequencing (Society for Immunotherapy of Cancer (SITC)).

10. McGranahan, N., Rosenthal, R., Hiley, C.T., Rowan, A.J., Watkins, T.B.K., Wilson, G.A., Birkbak, N.J., Veeriah, S., Van Loo, P., Herrero, J., and Swanton, C.; TRACERx Consortium (2017). Allele-specific HLA loss and immune escape in lung cancer evolution. Cell *171*, 1259–1271.e11. https://doi.org/10.1016/j.cell.2017.10.001.

11. Robinson, J., Soormally, A.R., Hayhurst, J.D., and Marsh, S.G.E. (2016). The IPD-IMGT/HLA Database - new developments in reporting HLA variation. Hum. Immunol. *77*, 233–237. https://doi.org/10.1016/j.humimm.2016.01.020.

12. Hilton, H.G., and Parham, P. (2013). Direct binding to antigen-coated beads refines the specificity and cross-reactivity of four monoclonal antibodies that recognize polymorphic epitopes of HLA class I molecules. Tissue Antigens *81*, 212–220. https://doi.org/10.1111/tan.12095.

13. Parham, P., and Bodmer, W.F. (1978). Monoclonal antibody to a human histocompatibility alloantigen, HLA-A2. Nature *276*, 397–399. https://doi.org/10.1038/276397a0.

14. Ying, T., Chen, W., Gong, R., Feng, Y., and Dimitrov, D.S. (2012). Soluble monomeric IgG1 Fc. J. Biol. Chem. *287*, 19399–19408. https://doi.org/10.1074/jbc.M112.368647.

15. Chaudhury, S., Lyskov, S., and Gray, J.J. (2010). PyRosetta: a script-based interface for implementing molecular modeling algorithms using Rosetta. Bioinformatics *26*, 689–691. https://doi.org/10.1093/bioinformatics/btq007.

16. Lefranc, M.P., Giudicelli, V., Duroux, P., Jabado-Michaloud, J., Folch, G., Aouinti, S., Carillon, E., Duvergey, H., Houles, A., Paysan-Lafosse, T., et al. (2015). IMGT(R), the international ImMunoGeneTics information system(R) 25 years on. Nucleic Acids Res. *43*, D413–D422. https://doi.org/10.1093/nar/gku1056.

17. Riley, T.P., Ayres, C.M., Hellman, L.M., Singh, N.K., Cosiano, M., Cimons, J.M., Anderson, M.J., Piepenbrink, K.H., Pierce, B.G., Weng, Z., and Baker, B.M. (2016). A generalized framework for computational design and mutational scanning of T-cell receptor binding interfaces. Protein Eng. Des. Sel. *29*, 595–606. https://doi.org/10.1093/protein/gzw050.

18. Xu, H., Hamburger, A.E., Mock, J.Y., Wang, X., Martin, A.D., Tokatlian, T., Oh, J., Daris, M.E., Negri, K.R., Gabrelow, G.B., et al. (2020). Structure-function relationships of chimeric antigen receptors in acute T cell responses to antigen. Mol. Immunol. *126*, 56–64. https://doi.org/10.1016/j.molimm.2020.07.020.

19. Wang, X., Wong, L.M., McElvain, M.E., Martire, S., Lee, W.H., Li, C.Z., Fisher, F.A., Maheshwari, R.L., Wu, M.L., Imun, M.C., et al. (2022). A rational approach to assess off-target reactivity of a dual-signal integrator for T cell therapy. Toxicol. Appl. Pharmacol. *437*, 115894. https://doi.org/10.1016/j.taap.2022.115894.

20. Aarnoudse, C.A., Krüse, M., Konopitzky, R., Brouwenstijn, N., and Schrier, P.I. (2002). TCR reconstitution in Jurkat reporter cells facilitates the identification of novel tumor antigens by cDNA expression cloning. Int. J. Cancer *99*, 7–13. https://doi.org/10.1002/ijc.10317.

21. Barnstable, C.J., Bodmer, W.F., Brown, G., Galfre, G., Milstein, C., Williams, A.F., and Ziegler, A. (1978). Production of monoclonal antibodies to group A erythrocytes, HLA and other human cell surface antigens-new tools for genetic analysis. Cell *14*, 9–20. https://doi.org/10.1016/0092-8674(78)90296-9.

22. Fierle, J.K., Abram-Saliba, J., Atsaves, V., Brioschi, M., de Tiani, M., Reichenbach, P., Irving, M., Coukos, G., and Dunn, S.M. (2022). A cell-based phenotypic library selection and screening approach for the de novo discovery of novel functional chimeric antigen receptors. Sci. Rep. *12*, 1136. https://doi.org/10.1038/s41598-022-05058-5.

23. Hudecek, M., Lupo-Stanghellini, M.T., Kosasih, P.L., Sommermeyer, D., Jensen, M.C., Rader, C., and Riddell, S.R. (2013). Receptor affinity and extracellular domain modifications affect tumor recognition by ROR1-specific chimeric antigen receptor T cells. Clin. Cancer Res. *19*, 3153–3164. https://doi.org/10.1158/1078-0432.CCR-13-0330.

24. Kabsch, W. (2010). Xds. Acta Crystallogr. D Biol. Crystallogr. *66*, 125–132. https://doi.org/10.1107/S0907444909047337.

25. Winn, M.D., Ballard, C.C., Cowtan, K.D., Dodson, E.J., Emsley, P., Evans, P.R., Keegan, R.M., Krissinel, E.B., Leslie, A.G.W., McCoy, A., et al. (2011). Overview of the CCP4 suite and current developments. Acta Crystallogr. D Biol. Crystallogr. *67*, 235–242. https://doi.org/10.1107/S0907444910045749.

26. McCoy, A.J., Grosse-Kunstleve, R.W., Adams, P.D., Winn, M.D., Storoni, L.C., and Read, R.J. (2007). Phaser crystallographic software. J. Appl. Crystallogr. *40*, 658–674. https://doi.org/10.1107/S0021889807021206.

27. Bunkóczi, G., and Read, R.J. (2011). Improvement of molecular-replacement models with Sculptor. Acta Crystallogr. D Biol. Crystallogr. *67*, 303–312. https://doi.org/10.1107/S0907444910051218.

28. Adams, P.D., Afonine, P.V., Bunkóczi, G., Chen, V.B., Davis, I.W., Echols, N., Headd, J.J., Hung, L.W., Kapral, G.J., Grosse-Kunstleve, R.W., et al. (2010). PHENIX: a comprehensive Python-based system for macromolecular structure solution. Acta Crystallogr. D Biol. Crystallogr. *66*, 213–221. https://doi.org/10.1107/S0907444909052925.

29. Emsley, P., Lohkamp, B., Scott, W.G., and Cowtan, K. (2010). Features and development of Coot. Acta Crystallogr. D Biol. Crystallogr. *66*, 486–501. https://doi.org/10.1107/S0907444910007493.

30. Alford, R.F., Leaver-Fay, A., Jeliazkov, J.R., O'Meara, M.J., DiMaio, F.P., Park, H., Shapovalov, M.V., Renfrew, P.D., Mulligan, V.K., Kappel, K., et al. (2017). The Rosetta all-atom energy function for macromolecular modeling and design. J. Chem. Theor. Comput. *13*, 3031–3048. https://doi.org/10.1021/acs.jctc.7b00125.